

MICROCOPY RESOLUTION TEST CHART
NATIONAL BUREAU OF STANDARDS - 1963 - A

62

NRL Memorandum Report 5673

AD-A161 697

Dynamics of the Large Scale Return Currents on Auroral Field Lines

SUPRIYA B. GANGULI AND H. G. MITCHELL, JR.

*Science Applications International Corporation
McLean, VA 22102*

P. J. PALMADESSO

*Geophysical and Plasma Dynamics Branch
Plasma Physics Division*

November 11, 1985

This research was sponsored by the Office of Naval Research
and the National Aeronautics and Space Administration.



SELECTED
NOV 25 1985
A

NAVAL RESEARCH LABORATORY
Washington, D.C.

DTIC FILE COPY

Approved for public release; distribution unlimited

71 20-85 022

REPORT DOCUMENTATION PAGE				
1a REPORT SECURITY CLASSIFICATION UNCLASSIFIED		1b REPORT SECURITY CLASSIFICATION AD-A161697		
2a SECURITY CLASSIFICATION AUTHORITY		3 DISTRIBUTION / AVAILABILITY OF REPORT Approved for public release; distribution unlimited.		
2b DECLASSIFICATION / DOWNGRADING SCHEDULE				
4 PERFORMING ORGANIZATION REPORT NUMBER(S) NRL Memorandum Report 5673		5 MONITORING ORGANIZATION REPORT NUMBER(S)		
6a NAME OF PERFORMING ORGANIZATION Naval Research Laboratory	6b OFFICE SYMBOL (if applicable) Code 4780	7a NAME OF MONITORING ORGANIZATION		
6c ADDRESS (City, State, and ZIP Code) Washington, DC 20375-5000		7b ADDRESS (City, State, and ZIP Code)		
8a NAME OF FUNDING / SPONSORING ORGANIZATION NASA and ONR	8b OFFICE SYMBOL (if applicable)	9 PROCUREMENT INSTRUMENT IDENTIFICATION NUMBER		
8c ADDRESS (City, State, and ZIP Code) Washington, DC 20546 Arlington, VA 22217		10 SOURCE OF FUNDING NUMBERS		
		PROGRAM ELEMENT NO (See page ii)	PROJECT NO	TASK NO. WORK UNIT ACCESSION NO
11 TITLE (Include Security Classification) Dynamics of the Large Scale Return Currents on Auroral Field Lines				
12 PERSONAL AUTHOR(S) Ganguli, Supriya B.,* Mitchell, H.G., Jr.,* and Palmadesso, P.J.				
13a TYPE OF REPORT Interim	13b TIME COVERED FROM _____ TO _____	14 DATE OF REPORT (Year, Month, Day) 1985 November 11	15 PAGE COUNT 43	
16 SUPPLEMENTARY NOTATION *Science Applications International Corporation, McLean, VA 22102 (Continues)				
17 COSATI CODES		18 SUBJECT TERMS (Continue on reverse if necessary and identify by block number)		
FIELD	GROUP	SUB-GROUP		
		> 13-moment system of transport equations Temperature anisotropy Return currents		
19 ABSTRACT (Continue on reverse if necessary and identify by block number) Multimoment fluid plasma simulations have been performed to study the dynamics of auroral field lines in the presence of large scale field-aligned return currents. The flux tube plasma has a rapid initial response to the onset of current. Electron velocity increases with the application of return current to the system. Electron temperature exhibits adiabatic cooling and temperature anisotropy but the electrons cool much more compared to their polar wind value. We have only considered cold ionospheric electrons in this simulation. The hydrogen ion drift velocity decreases and hydrogen ion temperature increases. The hydrogen ion temperature still exhibits the polar wind characteristics, i.e., the increase in temperature at the lower end of the tube, temperature anisotropy and adiabatic cooling.				
20 DISTRIBUTION / AVAILABILITY OF ABSTRACT <input checked="" type="checkbox"/> UNCLASSIFIED/UNLIMITED <input type="checkbox"/> SAME AS RPT <input type="checkbox"/> DTIC USERS		21 ABSTRACT SECURITY CLASSIFICATION UNCLASSIFIED		
22a NAME OF RESPONSIBLE INDIVIDUAL J. D. Huba		22b TELEPHONE (Include Area Code) (202) 767-3630	22c OFFICE SYMBOL Code 4780	

10. SOURCE OF FUNDING NUMBERS

PROGRAM ELEMENT NO.	PROJECT NO.	TASK NO.	WORK UNIT ACCESSION NO.
61153N	RR033-02-44	W-15494	DN430-607 DN380-475

16. SUPPLEMENTARY NOTATION (Continued)

This research was sponsored by the Office of Naval Research and the National Aeronautics and Space Administration.

CONTENTS

I. INTRODUCTION	1
II. THE MODEL	2
III. SIMULATIONS AND RESULTS	6
i. Polar Wind Simulation	6
ii. Return Current Simulation	8
IV. DISCUSSIONS AND SUMMARY	11
ACKNOWLEDGMENTS	11
REFERENCES	31
APPENDIX	33

Accession For	
NTIS CRA&I	<input type="checkbox"/>
DTIC TAB	<input type="checkbox"/>
Unannounced	<input type="checkbox"/>
Justification	
By	
Distribution/	
Availability Codes	
Dist	Availability or Special
A-1	



DYNAMICS OF THE LARGE SCALE RETURN CURRENTS ON AURORAL FIELD LINES

I. INTRODUCTION

The behavior of plasma on the auroral magnetic field lines has been the subject of a number of studies in recent years. Theoretical models of the polar wind (current free cases) have been developed by Banks and Holzer [1968, 1969], Holzer et al. [1971], Lemaire and Scherer [1973], and Schunk and Watkins [1981, 1982]. Using the 13-moment system of transport equations of Shunk [1977], Schunk and Watkins [1981, 1982] have studied the steady state flow of a fully ionized $H^+ - O^+ -$ electron plasma along geomagnetic field lines.

Using the same 13-moment system of equations, Mitchell and Palmadesso [1983] developed a dynamic numerical model of the plasma along an auroral field line. The plasma consists of the electrons, hydrogen and oxygen ions. The electrons and the hydrogen ions are the dynamic species in the model. They have performed simulations for the case of a current-free polar wind and the case in which an upward field aligned current was applied along the field line.

However, there has been some recent interest concerning the return currents which motivated us to undertake a numerical study using a computer simulation to investigate the dynamics of the large scale return currents on the auroral field lines. The field aligned return currents flow from the magnetosphere to the ionosphere and are carried by cold electrons of ionospheric origin. It is now well established that the field aligned currents play an important role in the magnetosphere-ionosphere coupling process. In terms of region 1/region 2 large scale field aligned current systems [Iijima and Potemra, 1976] large scale return currents are

Manuscript approved August 12, 1985.

identified as region 1 at the morning sector and region 2 at the evening sector. The typical value of this current-system varies usually from $1.0 \mu\text{A}/\text{m}^2$ to $2.0 \mu\text{A}/\text{m}^2$. Within the region 1/region 2 current system, small-scale distributions of both upward and downward currents are observed in association with auroral arcs.

We have performed simulations to study the dynamics of the large scale return currents on auroral field lines, using the dynamic numerical model of Mitchell and Palmadesso [1983]. The model is a multi-moment approximation of plasma consisting of the electrons, hydrogen ions and oxygen ions along a segment of geomagnetic field line extending from an altitude of 800 km to 10 RE. We compared our results to those of Mitchell and Palmadesso [1983] to study the difference in dynamics of return currents versus upward currents and the current free polar wind case.

We are also interested in the dynamics of auroral field lines including the effects of anomalous transport processes such as anomalous resistivity and associated anisotropic heating. The work is in progress and will be the subject of a future report.

II. THE MODEL

The field line model of Mitchell and Palmadesso [1983] was designed to dynamically simulate the behavior of the plasma in a flux tube encompassing an auroral field line. The electrons and the hydrogen ions are the dynamic species in the model. The oxygen ions are a static background population

at a constant temperature. The model uses the 13-moment system of transport equations of Schunk [1977]. The distribution function is assumed to be gyrotropic about the field line direction, which reduces the 13-moment approximation to five moments. The five moments are number density, temperatures parallel and perpendicular to the field line, and species velocity and heat flow along the line. The resulting transport equations are as follows:

$$\frac{\partial n_s}{\partial t} = -v_s \frac{\partial n_s}{\partial r} - n_s \frac{\partial v_s}{\partial r} - \frac{n_s v_s}{A} \frac{\partial A}{\partial r} + \frac{\delta n_s}{\delta t} \quad (1)$$

$$\begin{aligned} \frac{\partial v_s}{\partial t} = & -v_s \frac{\partial v_s}{\partial r} - \frac{k}{m_s} \frac{\partial T_{s\parallel}}{\partial r} - \frac{k T_{s\parallel}}{m_s n_s} \frac{\partial n_s}{\partial r} - \frac{k(T_{s\parallel} - T_{s\perp})}{m_s A} \frac{\partial A}{\partial r} \\ & + \frac{e_s}{m_s} E - \frac{GM}{r^2} + \frac{\delta v_s}{\delta t} \end{aligned} \quad (2)$$

$$k \frac{\partial T_{s\parallel}}{\partial t} = -v_s k \frac{\partial T_{s\parallel}}{\partial r} - 2k T_{s\parallel} \frac{\partial v_s}{\partial r} - \frac{6}{5n_s} \frac{\partial q_s}{\partial r} - \frac{2}{5} \frac{q_s}{n_s A} \frac{\partial A}{\partial r} + k \frac{\delta T_{s\parallel}}{\delta t} \quad (3)$$

$$k \frac{\partial T_{s\perp}}{\partial t} = -v_s k \frac{\partial T_{s\perp}}{\partial r} - \frac{2}{5n_s} \frac{\partial q_s}{\partial r} - \left(\frac{4}{5} \frac{q_s}{n_s} + v_s k T_{s\perp} \right) \frac{1}{A} \frac{\partial A}{\partial r} + k \frac{\delta T_{s\perp}}{\delta t} \quad (4)$$

$$\begin{aligned}
\frac{\partial q_s}{\partial t} = & -v_s \frac{\partial q_s}{\partial r} - \frac{16}{5} q_s \frac{\partial v_s}{\partial r} - \left(\frac{11}{18} T_{s\parallel} + \frac{8}{9} T_{s\perp} \right) \frac{n_s k^2}{m_s} \frac{\partial T_{s\parallel}}{\partial r} \\
& - \left(\frac{17}{9} T_{s\parallel} - \frac{8}{9} T_{s\perp} \right) \frac{n_s k^2}{m_s} \frac{\partial T_{s\perp}}{\partial r} + \frac{4k^2}{9m_s} (T_{s\parallel} - T_{s\perp})^2 \frac{\partial n_s}{\partial r} \\
& + \left[\frac{n_s k^2}{m_s} (T_{s\parallel} - T_{s\perp}) \left(\frac{1}{3} T_{s\parallel} - \frac{4}{3} T_{s\perp} \right) - \frac{7}{5} v_s q_s \right] \frac{1}{A} \frac{\partial A}{\partial r} + \frac{\delta q_s}{\delta t}
\end{aligned} \tag{5}$$

where, n_s is the number density of the species s ,

v_s is the velocity,

$T_{s\parallel}$ is the parallel temperature,

$T_{s\perp}$ is the perpendicular temperature,

q_s is the heat flow,

m_s is the mass,

e_s is the charge of species s ,

A is the cross-sectional area of the flux tube,

E is the electric field parallel to the field line,

k is Boltzmann's constant,

G is the gravitational constant and

M is the mass of the earth.

The collision terms used in the present simulation are Burgers' [1979] collision terms for the case of Coulomb collisions with corrections for

finite species' velocity differences, and are given in Appendix I.

The scale of this model is large compared to the electron Debye length, so the transport equation (1) for electron number density may be replaced by an expression for charge neutrality:

$$n_e = n_p + n_o \quad (6)$$

We have assumed that the total flux tube current I remains constant

$$I = eA(n_p v_p - n_e v_e) \quad (7)$$

which implies,

$$v_e = \frac{1}{n_e} (n_p v_p - \frac{I}{eA}) \quad (8)$$

Using equations (2), (7) and (8) the electric field E parallel to the field line is calculated.

$$E = \frac{m_s}{en_e A} \frac{\partial}{\partial r} (n_p v_p^2 A - n_e v_e^2 A) - \frac{k}{e} \left[\frac{\partial T_{e\parallel}}{\partial r} + \frac{T_{e\parallel}}{n_e} \frac{\partial n_e}{\partial r} + \frac{(T_{e\parallel} - T_{e\perp})}{A} \frac{\partial A}{\partial r} \right] - \frac{n_o m GM}{n_e r^2} + \frac{m}{e} \left[\frac{\delta v_e}{\delta t} - \frac{n_p}{n_e} \frac{\delta v_p}{\delta t} \right], \quad (9)$$

III. SIMULATIONS AND RESULTS

In order to perform the field aligned current simulation we have to perform the current free polar wind simulation first to be used as the initial steady state of the flux tube. This was also done by Mitchell and Palmadesso and will be described briefly here.

i. Polar Wind Simulation (Zero Current)

The polar wind simulation was carried out for a current-free case. The lower boundary is fixed at 800 km. The simulation was carried up to an altitude of 10 RE on an unequally spaced grid. The cell size is small at the lower end of the field line in order to study the transport effects in the presence of the large density gradients due to the small scale height of oxygen and satisfy stability conditions. The flux tube plasma consisting of the hydrogen ions, oxygen ions and the electrons was initialized at a constant temperature of 2000^oK. The initial conditions used are those of Mitchell and Palmadesso [1983].

In the polar wind, the hydrogen ions are accelerated upwards in the flux tube to supersonic velocities due to the flux tube divergence and the small partial pressure of H⁺ at the upper end of the field line. In steady state polar wind models the hydrogen ion velocity can be either subsonic or supersonic. To date only the supersonic polar wind has been observed. The oxygen ions are the dominant species up to an altitude of around 3500 km. The ambipolar electric field value produces the sharp increase in the

hydrogen ion velocity at the lower end of the flux tube. In the steady state the electrons and the hydrogen ions reach the same maximum velocity, as it is clear from equation (8). This is shown in figure (1b). The total flux along the flux tube is conserved, i.e., $nVA = \text{constant}$. Therefore, as the velocity and the area increase with altitude the density should decrease. The hydrogen ion density decreases as it flows through the diverging flux tube, shown in figure (1a). The electron density also decreases, due to charge neutrality equation (6) .

The hydrogen ion temperature (shown in figure 1c) exhibits three interesting characteristics:

- (1) The temperature increases at the lower end of the tube.
- (2) Adiabatic cooling - supersonic ion gas cools down as it expands in a diverging magnetic field.
- (3) Temperature anisotropy.

The temperature increase is caused by Joule heating of the hydrogen from collisions with the oxygen ions. This effect becomes weaker with increasing altitude due to small scale height of the oxygen. As a result, the hydrogen ion temperature profiles show an increase in temperature before it exhibits adiabatic cooling. The temperature anisotropy develops around 2500 km and is caused by the mirror effect where the perpendicular energy is transferred to the parallel energy.

The electron temperature profiles (shown in figure 1d) exhibit :

- (1) Adiabatic cooling,
- (2) Temperature anisotropy.

However, the latter effect is more prominent in the hydrogen ion temperature profiles. The electron thermal velocity is much higher than the electron bulk flow velocity, hence thermal conductivity is more

effective at reducing flow related temperature anisotropies and gradients for electrons.

It is also noted that when the drift velocity of the hydrogen ions is equal to that of electrons the hydrogen ions cool much more than the electrons. The hydrogen ion temperature profiles maintain significant gradients at high altitudes and exhibit large temperature anisotropies at the upper end of the flux tube.

Mitchell and Palmadesso [1983] compared the results of their polar wind simulation with the previous studies of the polar wind by Schunk and Watkins [1982] and Banks and Holzer [1971] and the results were found to be in good agreement.

ii. Return Current Simulation

In this section we discuss our results of the field aligned return current simulation and compare those with the polar wind (zero current) case as described in Section I and with the upward current case studied by Mitchell and Palmadesso [1983].

Using the polar wind simulation as the initial steady state of the flux tube, simulations were performed with return currents with a minimum value of $-1.0 \mu\text{A}/\text{m}^2$ and a peak value of $-2.0 \mu\text{A}/\text{m}^2$.

We will first discuss the case where a current of $-1.0 \mu\text{A}/\text{m}^2$ was applied. With the onset of the current the electron velocity increases with altitude (figure 2). The electron temperature profile still exhibits adiabatic cooling and temperature anisotropy, but since the electron velocity is much higher in this case as compared to the polar wind value,

the electrons cool much more rapidly with increasing altitude. The electron temperature gradient decreases. Notice that here we have only considered cold electrons of ionospheric origin, like Mitchell and Palmadesso [1983]. The electron temperature profiles are shown at time intervals of ten, thirty, fifty and seventy minutes on figures 3(a), 3(b) 3(c) and 3(d), where the response of electron temperature profiles with time are clearly observed. We compared our results with the upward current case of Mitchell and Palmadesso [1983] and notice that unlike the effects of return currents the application of upward current reduces the electron velocity and increases the total electron temperature. In the latter case the electrons are heated in the lower end of the flux tube and the temperature gradient results in a large upward electron heat flow and electron thermal wave propagating up the field line.

The electric field maintains the same profile as before but decreases in magnitude from the polar wind value thereby decreasing the hydrogen ion velocity. This is unlike the upward current case of Mitchell and Palmadesso [1983], where the ambipolar electric field increases by an order of magnitude accelerating the hydrogen ions upwards. The decrease in H^+ velocity causes a velocity ripple which in turn produces an H^+ density depletion and these propagate upwards through the flux tube as the simulation was carried on at later times. Due to the current conservation requirement, the electron velocity increases at the density depletion, and hence the upward propagating velocity ripple is also noticed in the electrons. This effect is clearly seen for times ten, thirty, fifty and seventy minutes after the onset of the current as shown in figures 2(a), 2(b), 2(c) and 2(d). After the velocity ripples pass through the flux tube, the electron velocity settles down at a lower value than before (but

much higher than the polar wind value) in order to maintain the current I constant. Also, the velocity of the hydrogen ions decreases at the upper end of the flux tube. As before the anisotropy of cooling is evident in the hydrogen ions but the hydrogen parallel and perpendicular temperatures increase as the H^+ ion velocity decreases. The ripple in velocity produces a ripple in the temperature which, like the velocity ripple, also flows up the flux tube with time. The hydrogen ion temperature profiles are shown on figures 4(a), 4(b), 4(c) and 4(d) at ten, thirty, fifty and seventy minutes after the onset of the current.

Simulations were then performed with higher currents up to a peak current of $-2.0 \mu A/m^2$. The electron velocity increases with the increase of current (shown in figure 5a), and the electron temperature still exhibits adiabatic cooling and temperature anisotropy (figure 5b). The ambipolar electric field decreases, further decreasing the H^+ velocity (figure 5a). Velocity ripples are observed as before and these propagate through the flux tube as seen in later runs (that is, ten, thirty, fifty and seventy minutes after the onset of this current). To conserve the current flowing in the system, the electron velocity decreases (after the ripple flows out through the tube) with the decrease in hydrogen ion velocity. However, compared to the previous case, the electron velocity still remains at a higher value, while the H^+ ion velocity decreases. The hydrogen ion temperature profile for this current is shown in figure 5(c).

IV. DISCUSSIONS AND SUMMARY

We have used a dynamic numerical model to investigate the plasma dynamics in the presence of large scale field aligned return currents. We have also compared our results with those of the current-free polar wind and upward current simulations.

The flux tube plasma has a rapid initial response to the onset of the current. The electron velocity and temperature have rapid response to sudden change in conditions with a time constant of about few minutes. Also, the behavior of the energy transport in the collisionless region determines the time scales on which the flux tube plasma reaches equilibrium.

In this paper we have only considered cold electrons of ionospheric origin. Similar studies of return currents using hot magnetospheric electrons at the upper boundary are in progress and will be the subject of a future report. Kindel and Kennel [1971] examined several current driven instabilities and showed that electrostatic ion cyclotron instability has the lowest threshold. Our simulations show that the electron drift velocity corresponding to a current of $-1.0 \mu\text{A}/\text{m}^2$ is above the threshold for electrostatic ion cyclotron waves. The effects of anomalous resistivity and anisotropic ion heating arising due to EIC instability will be discussed in a future article.

Acknowledgments

This work was supported by the Office of Naval Research and the National Aeronautics and Space Administration.

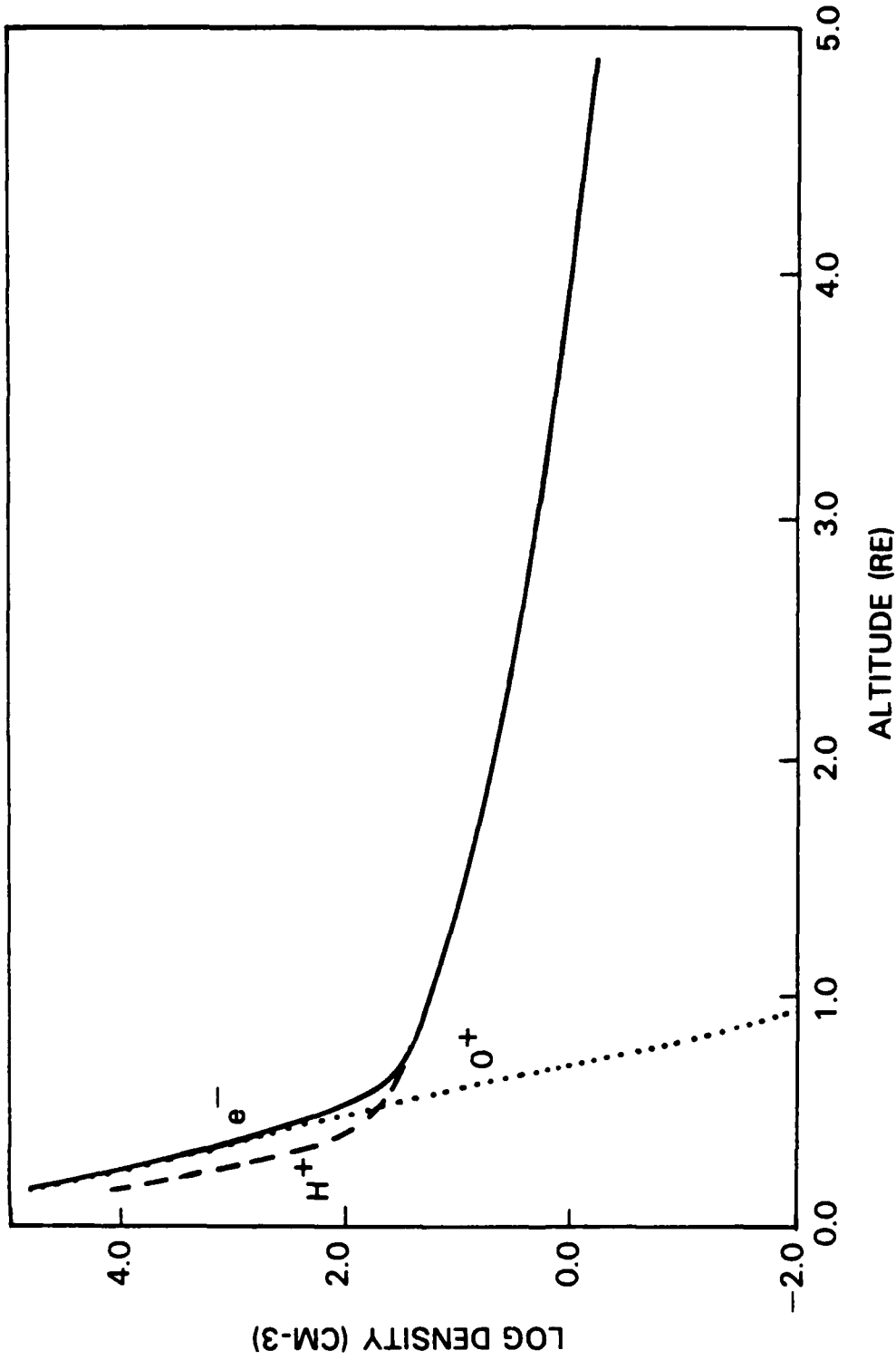


Figure 1. (a) Densities for the steady-state polar wind with no field-aligned current: electrons (solid curve), H⁺ (dashed curve), O⁺ (dotted curve).

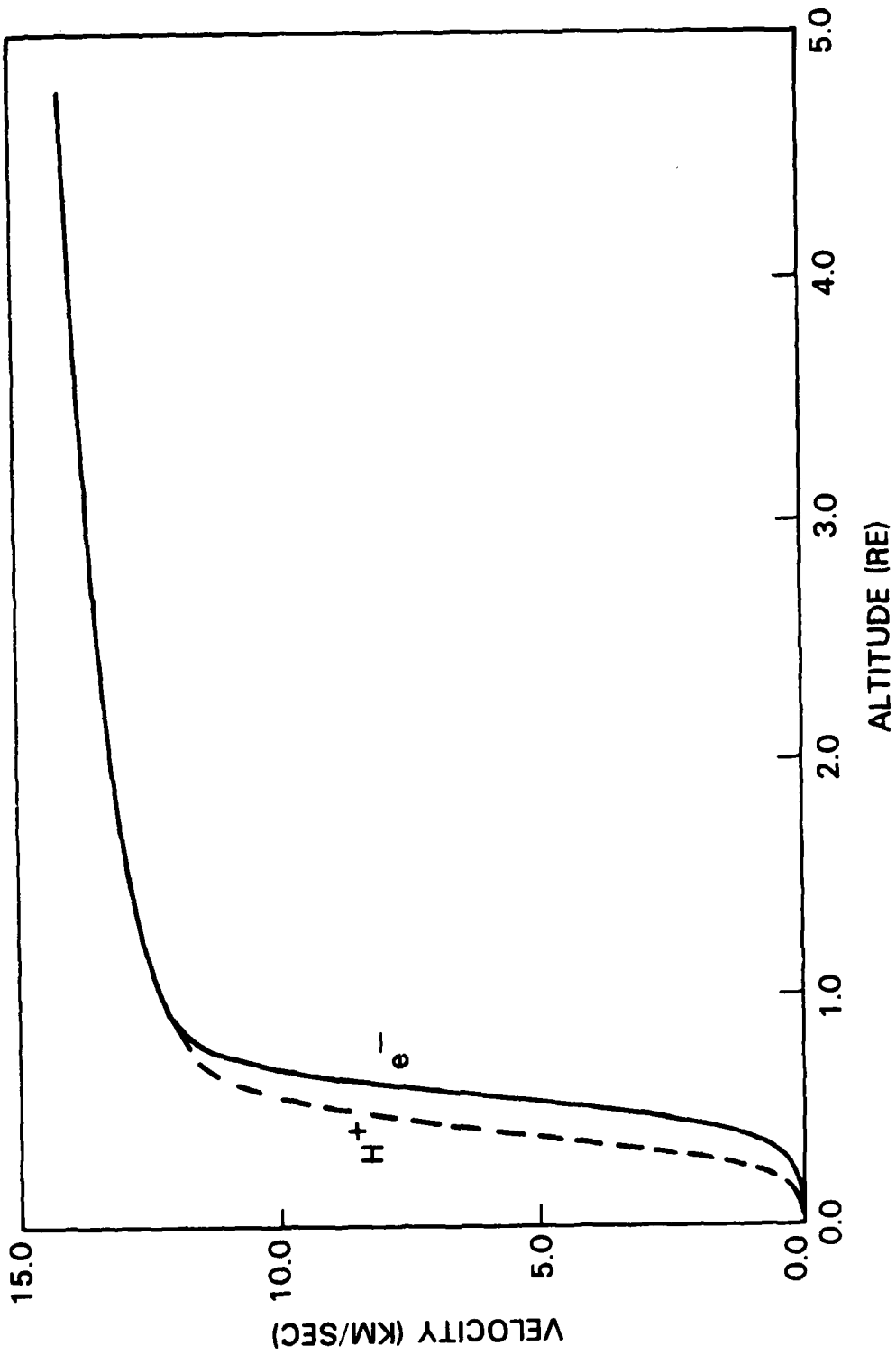


Figure 1. (b) Velocities for the steady-state polar wind with no field-aligned current: e^- (solid curve), H^+ (dashed curve). The oxygen ion velocity is uniformly zero.

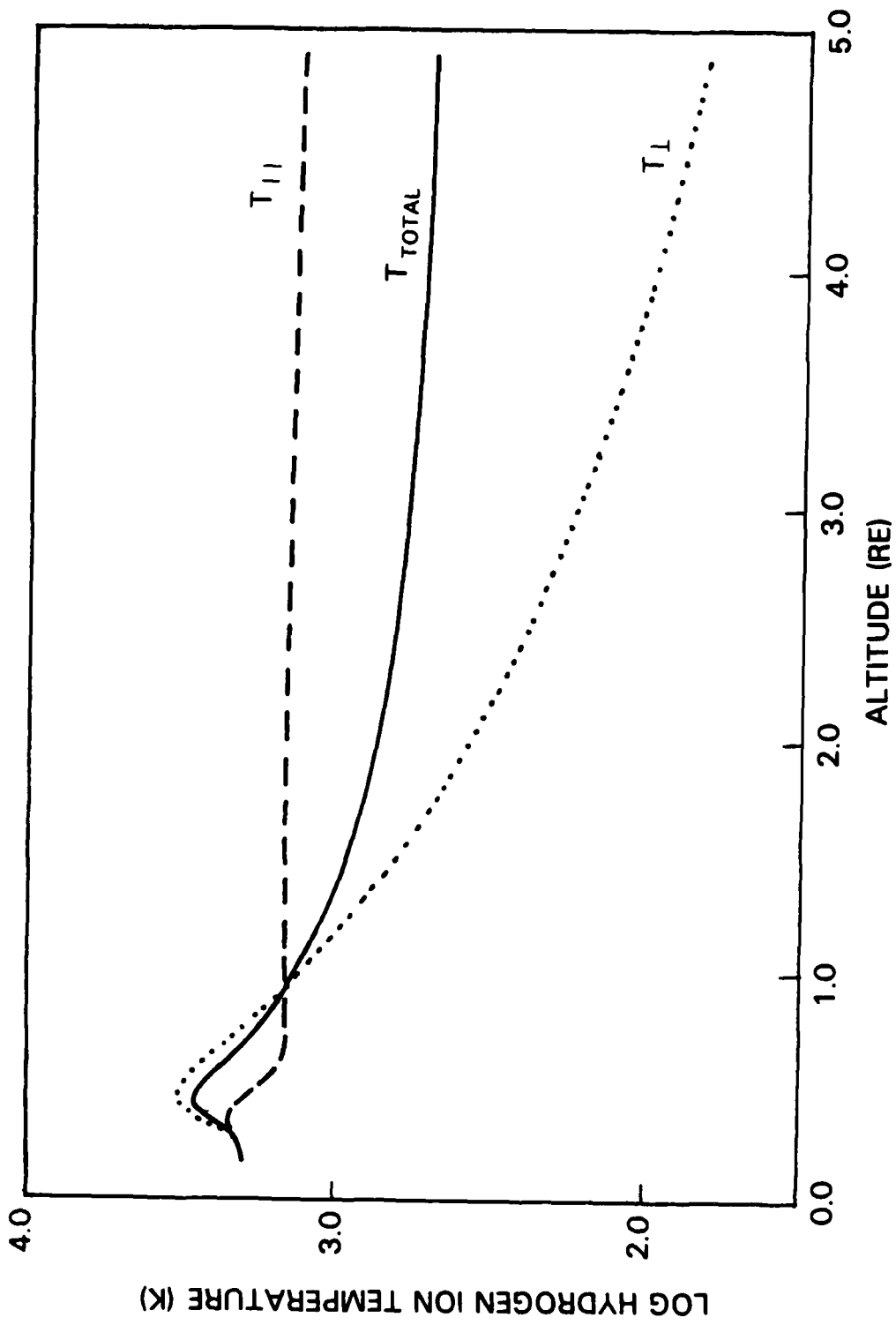


Figure 1. (c) Hydrogen ion temperatures for the steady-state polar wind with no field-aligned current: total temperature (solid curve), $T_{||}$ (dashed curve), T_{\perp} (dotted curve).

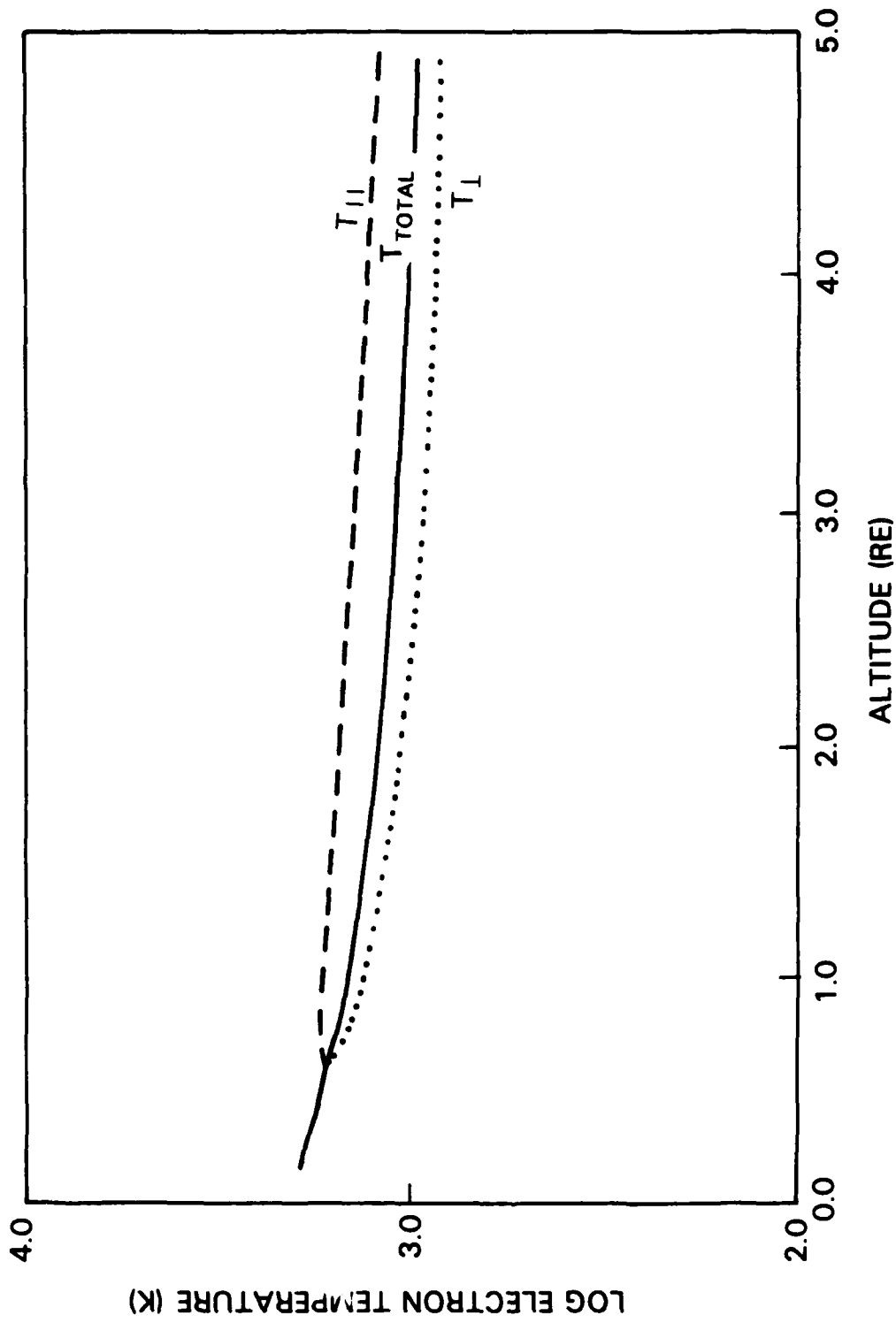


Figure 1. (d) Electron temperatures for the steady-state polar wind with no field-aligned current: total temperature (solid curve), $T_{||}$ (dashed curve), T_{\perp} (dotted curve).

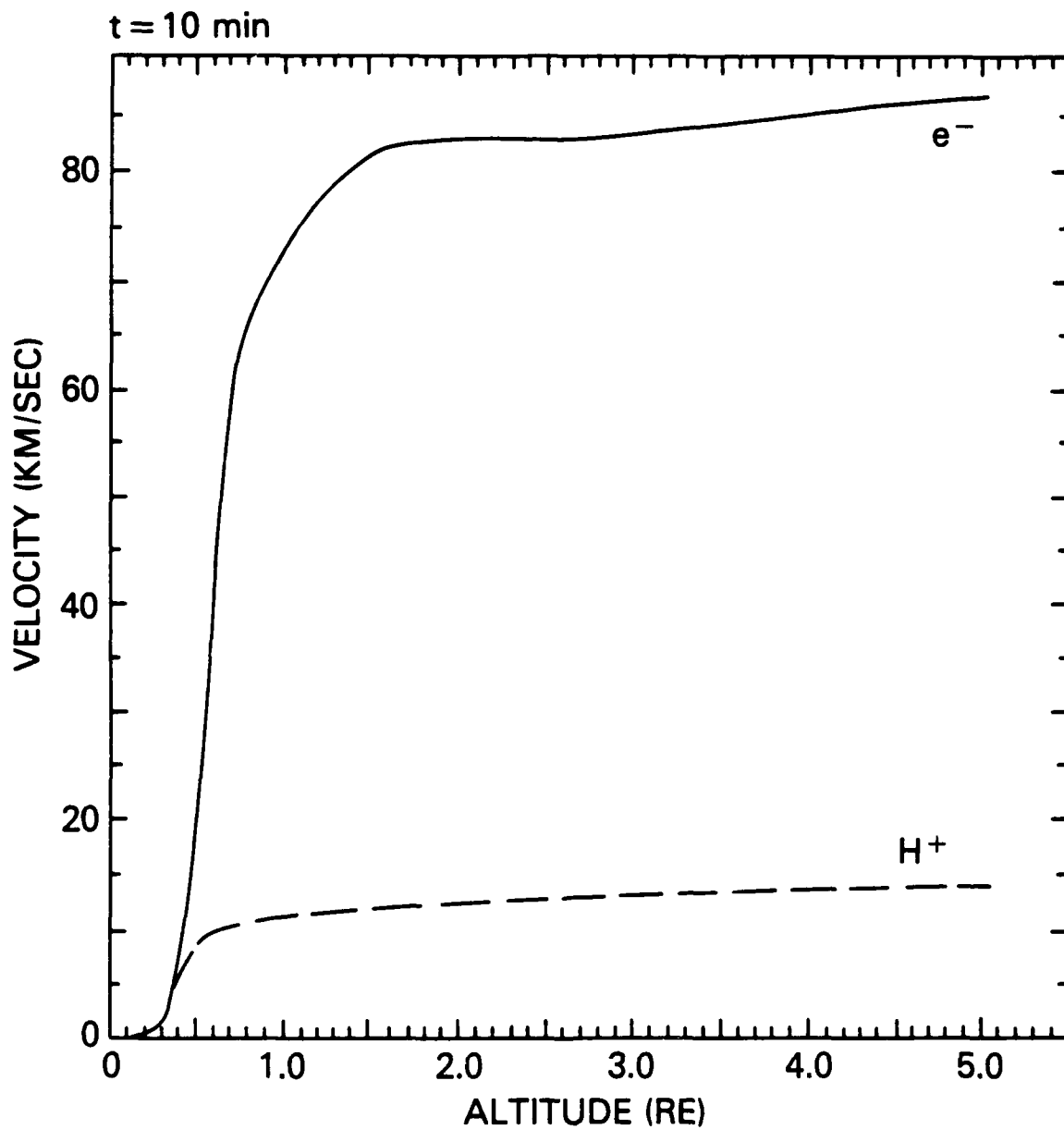


Figure 2. (a). Velocities after 10 minutes after the onset of a current of $-1.0 \mu\text{A}/\text{m}^2$ at 1500 km: e^- (solid curve), H^+ (dashed curve).

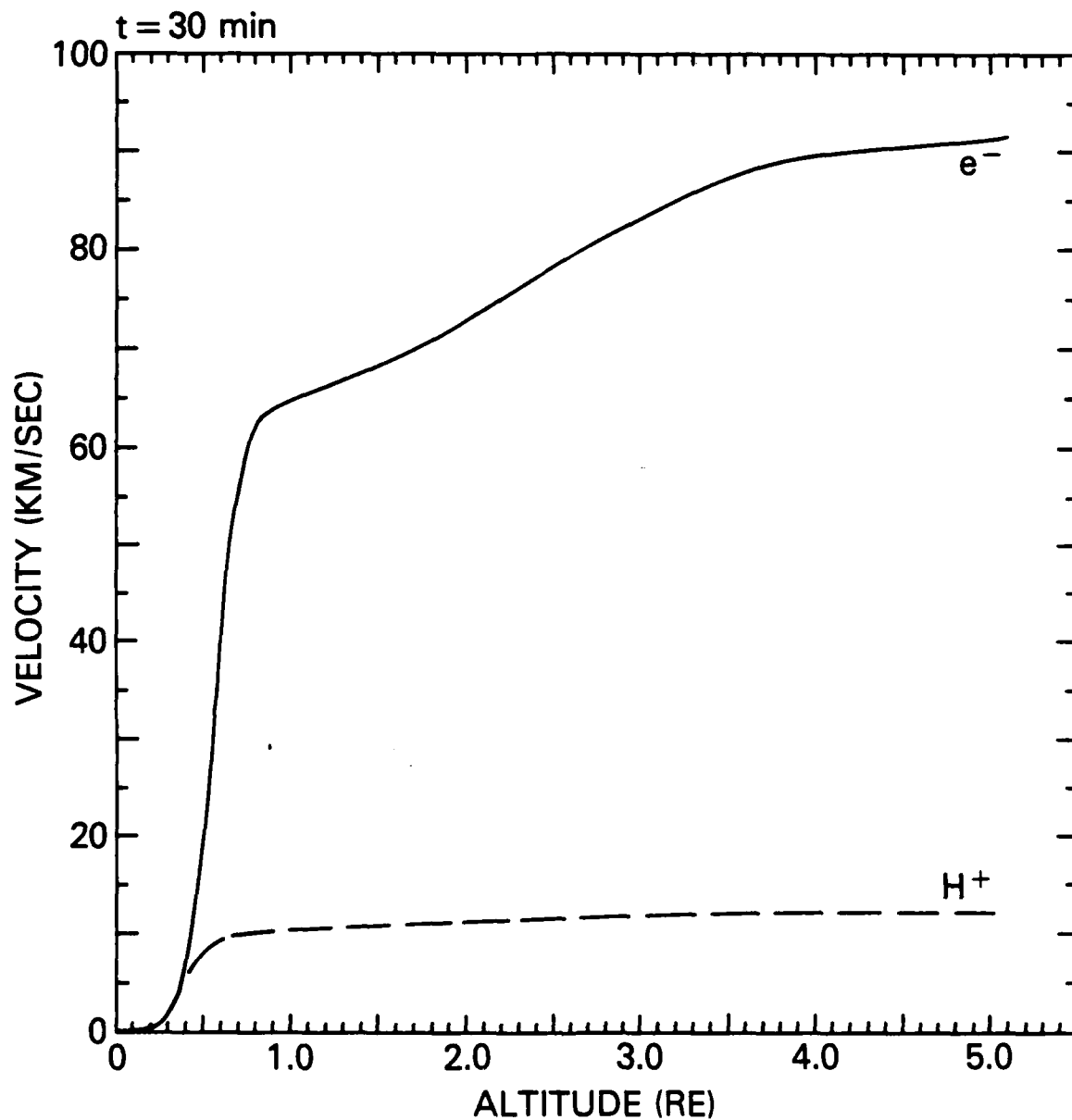


Figure 2. (b) Velocites after 30 minutes after the onset of a current of $-1.0 \mu\text{A}/\text{m}^2$ at 1500 km: e^- (solid curve), H^+ (dashed curve).

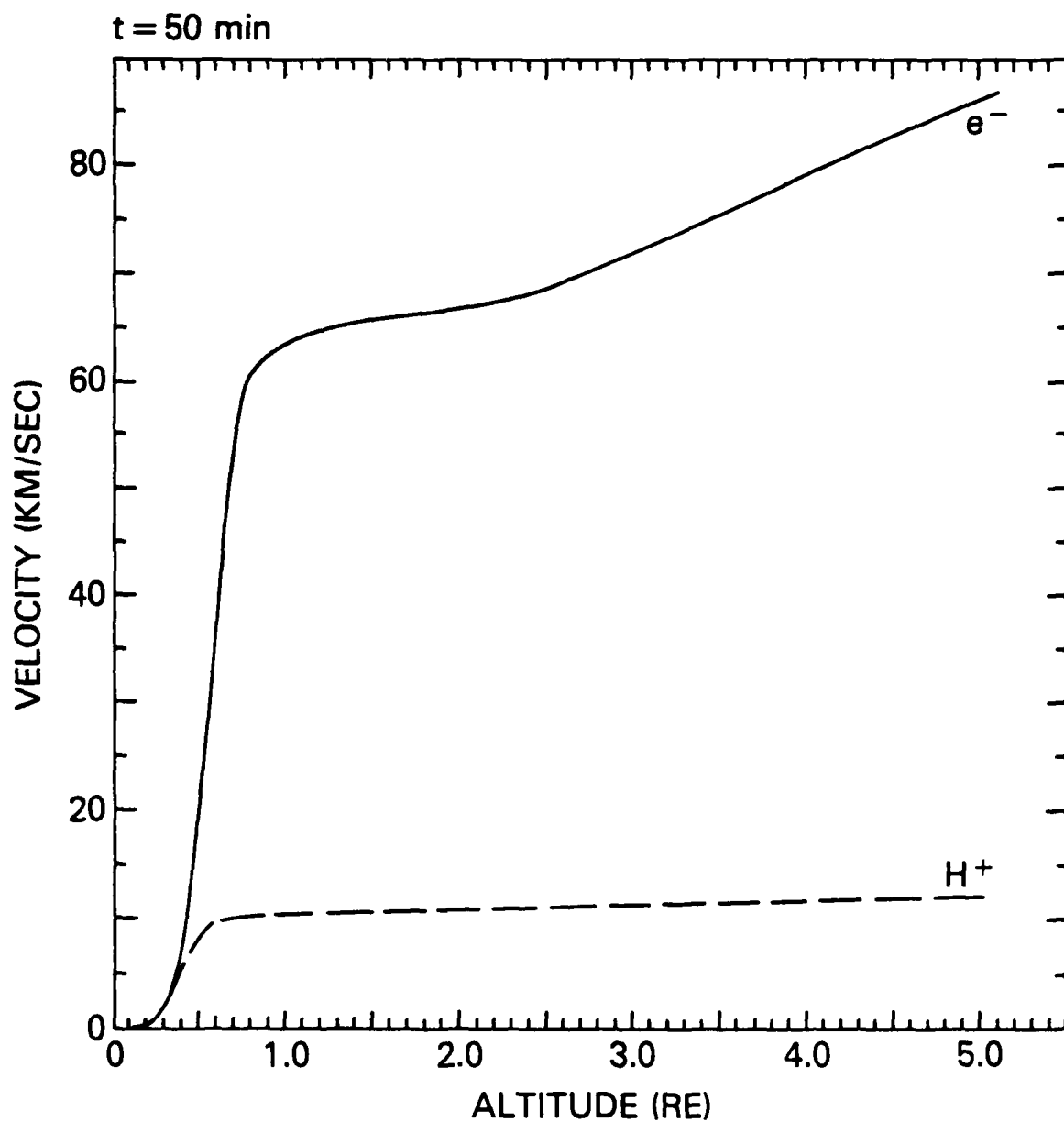


Figure 2. (c) Velocites after 50 minutes after the onset of a current of $-1.0 \mu\text{A}/\text{m}^2$ at 1500 km: e^- (solid curve), H^+ (dashed curve).

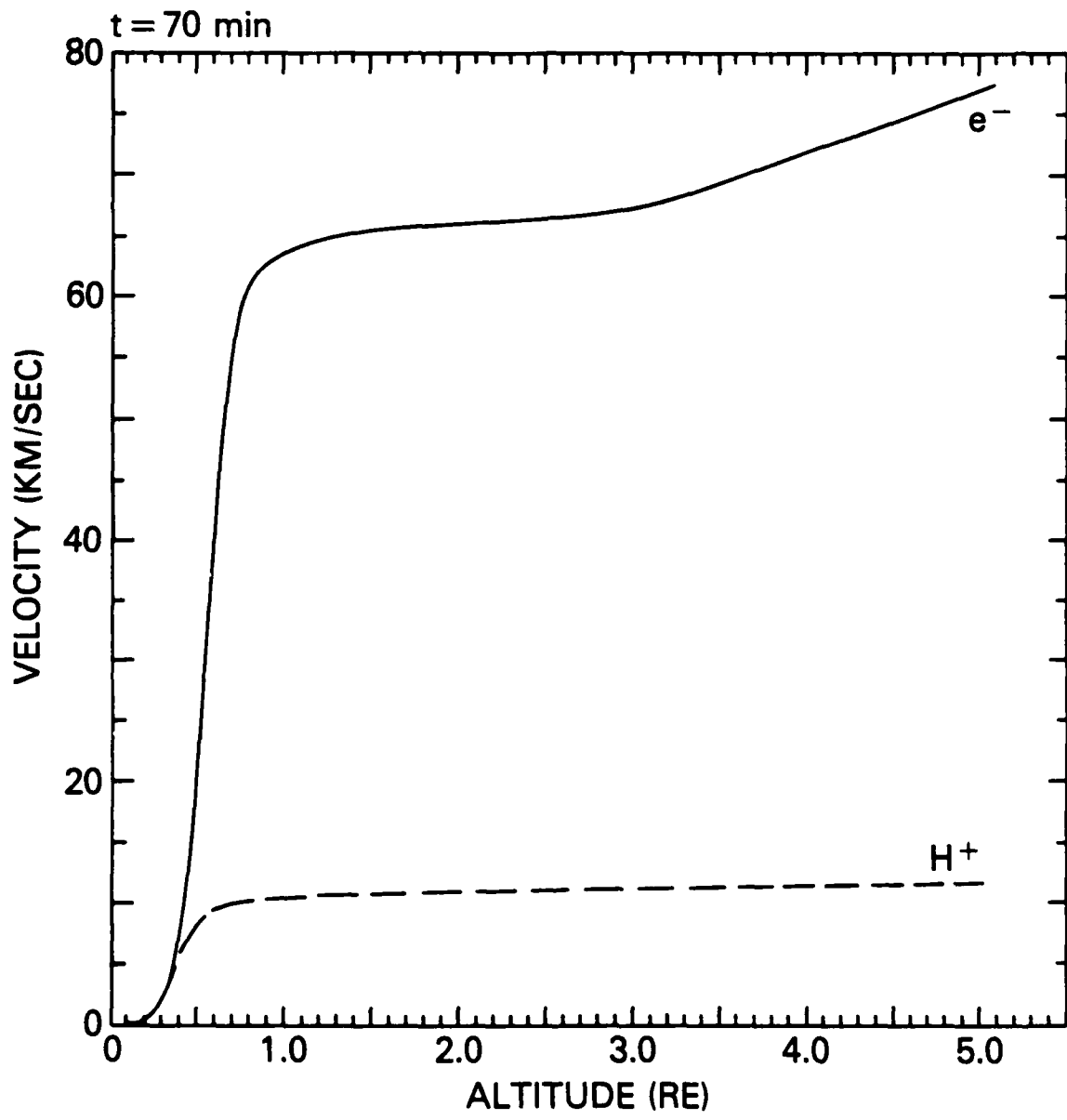


Figure 2. (d) Velocities after 70 minutes after onset of a current of $-1.0 \mu A/m^2$ at 1500 km: e^- (solid curve), H^+ (dashed curve).

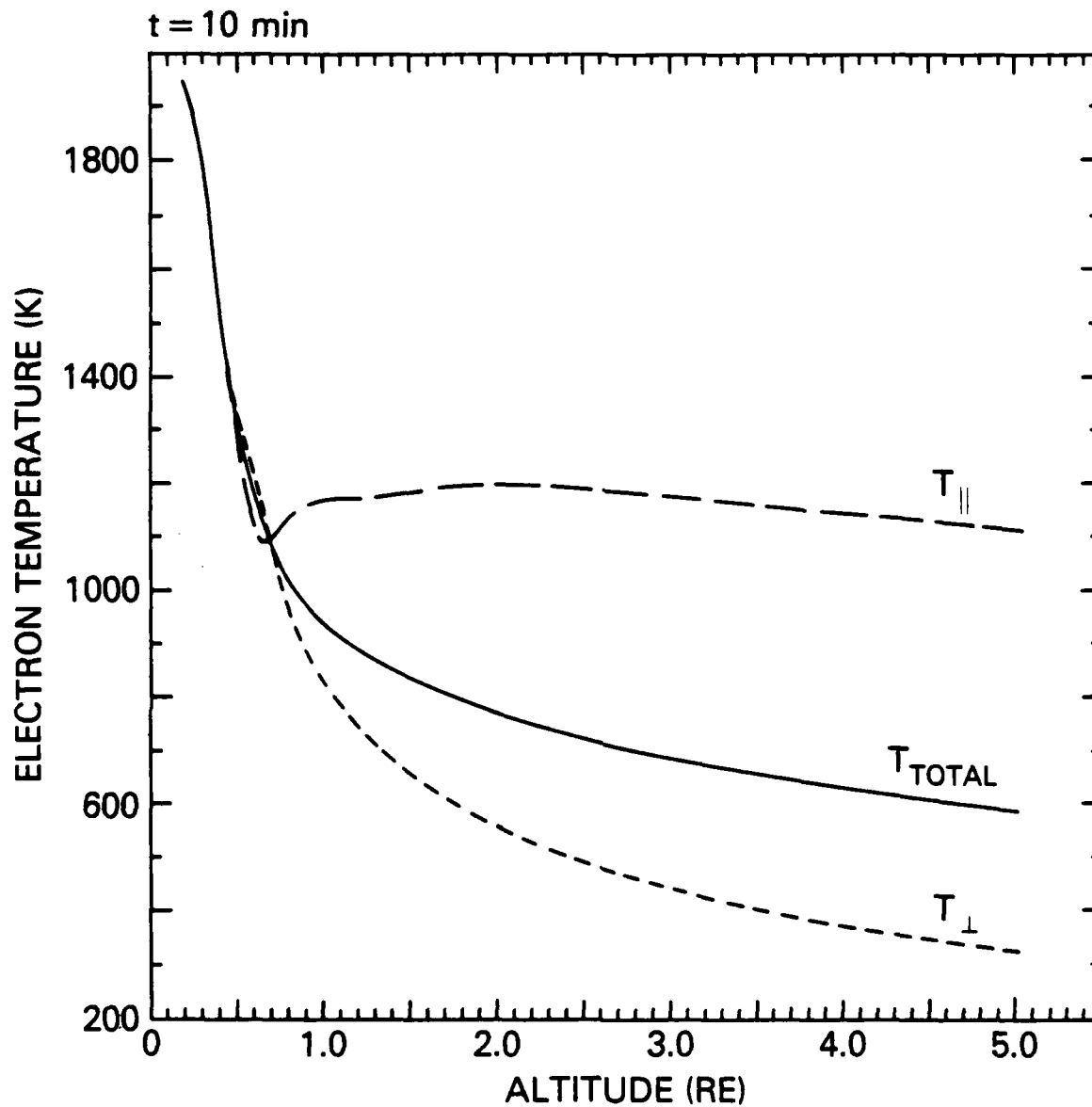


Figure 3. (a) Electron temperatures 10 minutes after the onset of a current of $-1.0 \mu\text{A}/\text{m}^2$ at 1500 km: total temperature (solid curve), T_{\parallel} (dashed curve), T_{\perp} (dotted curve).

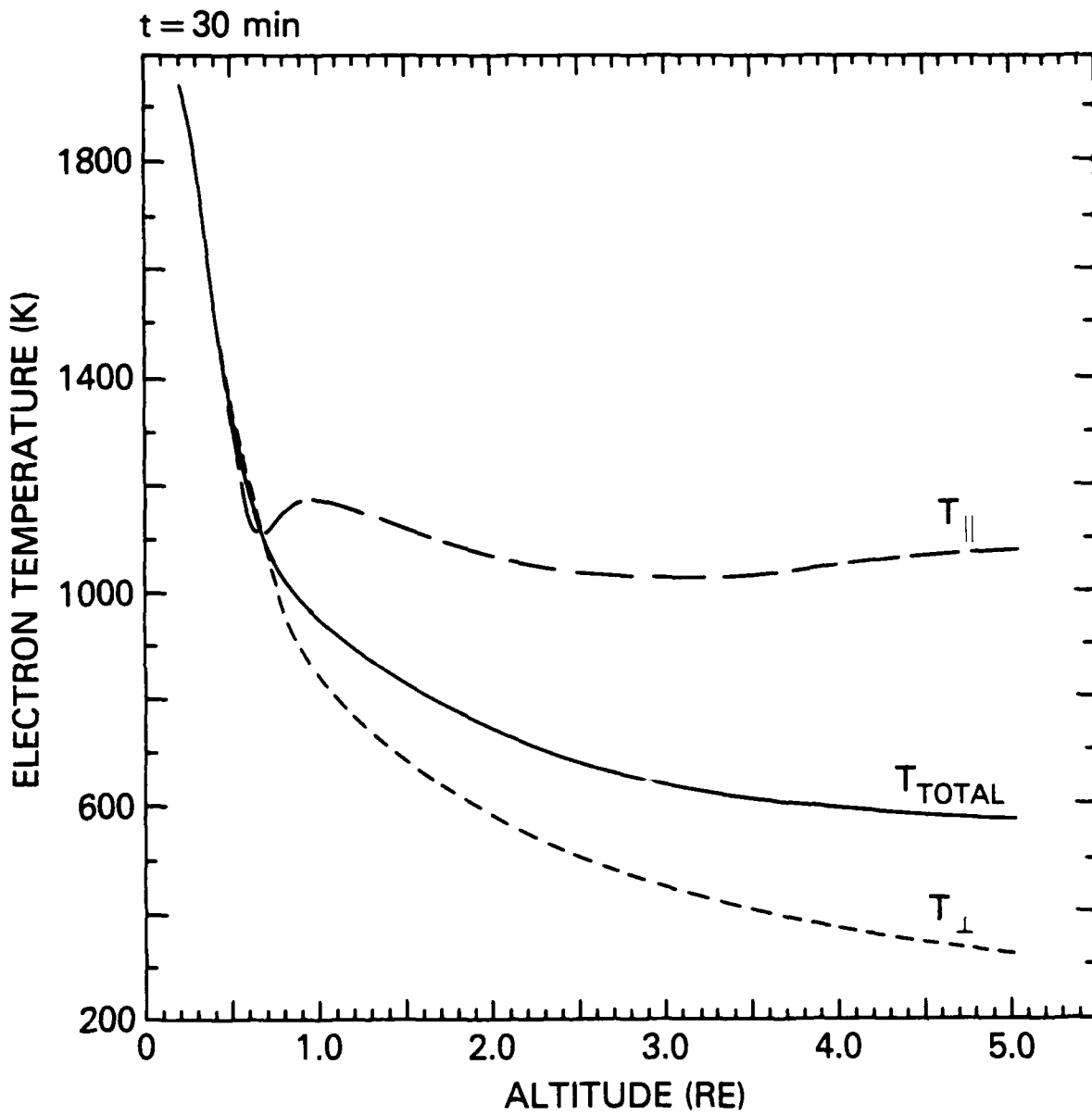


Figure 3. (b) Electron temperatures 30 minutes after onset of a current of $-1.0 \mu\text{A}/\text{m}^2$.

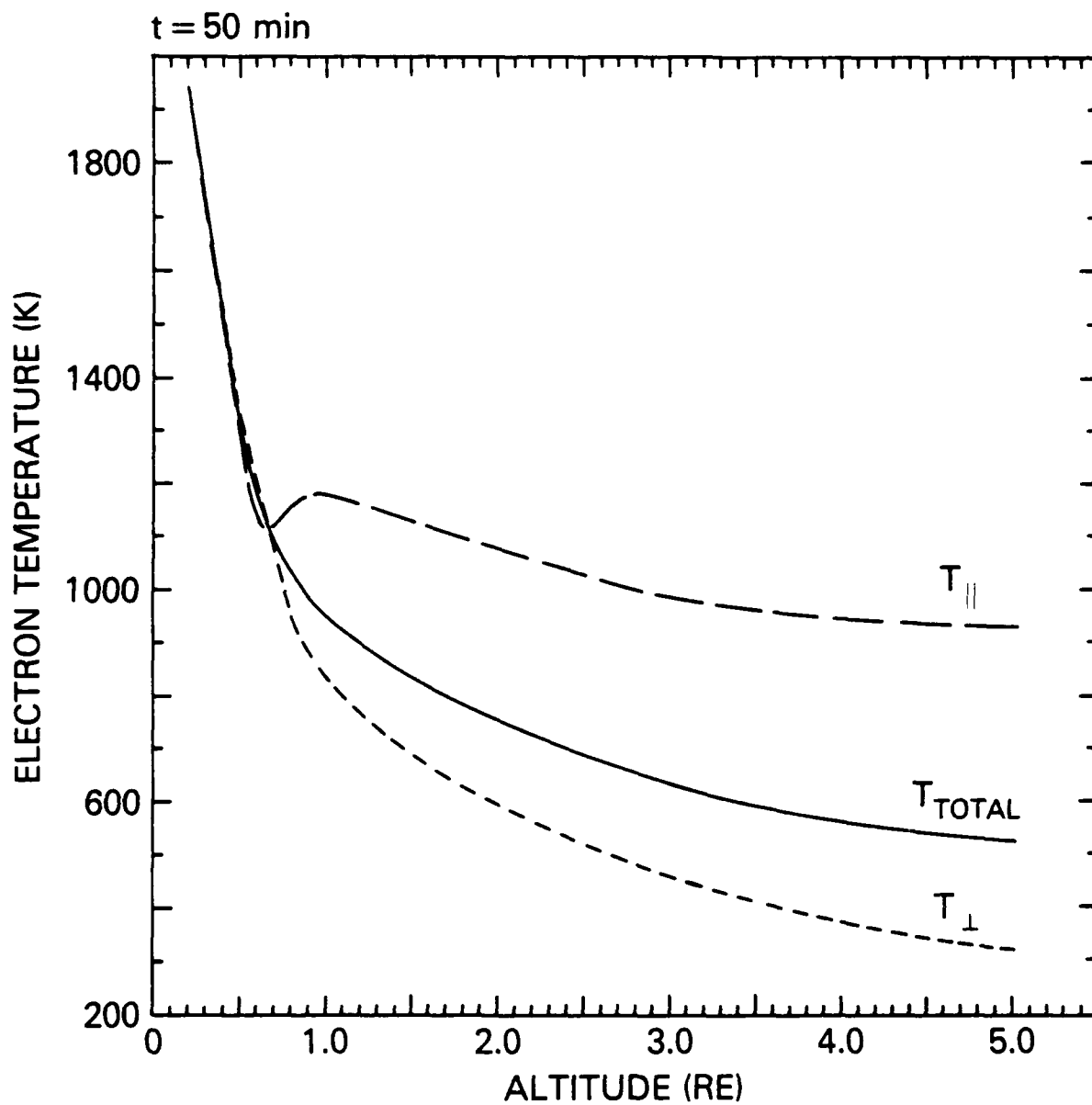


Figure 3. (c) Electron temperatures 50 minutes after onset of a current of $-1.0 \mu\text{A}/\text{m}^2$.

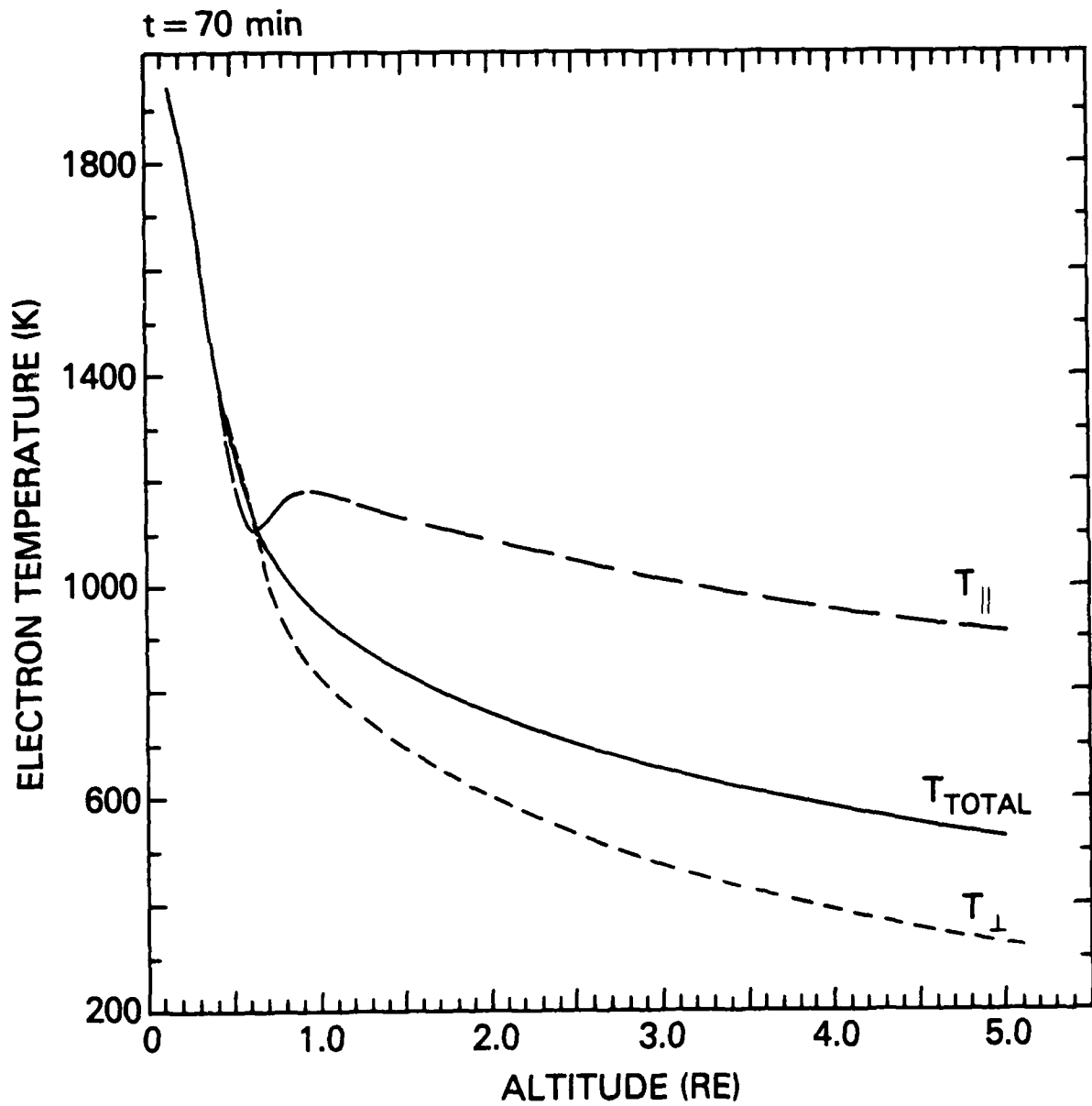


Figure 3. (d) Electron temperatures 70 minutes after onset of a current of $-1.0 \mu\text{A}/\text{m}^2$.

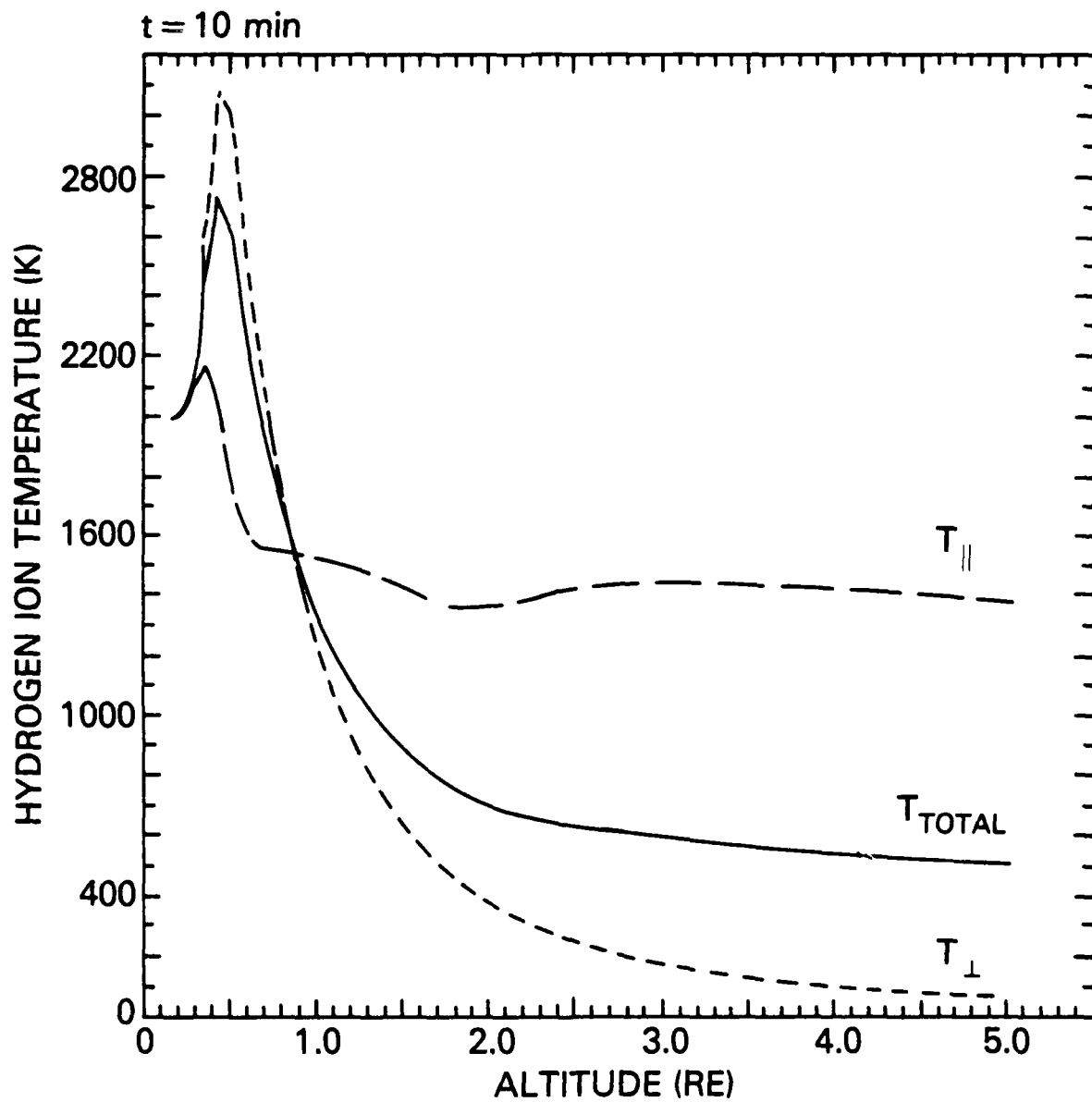


Figure 4. (a) Hydrogen ion temperatures 10 minutes after the onset of a current of $-1.0 \mu\text{A}/\text{m}^2$. 1500 km: total temperature (solid curve), T_{\parallel} (dashed curve), T_{\perp} (dotted curve).

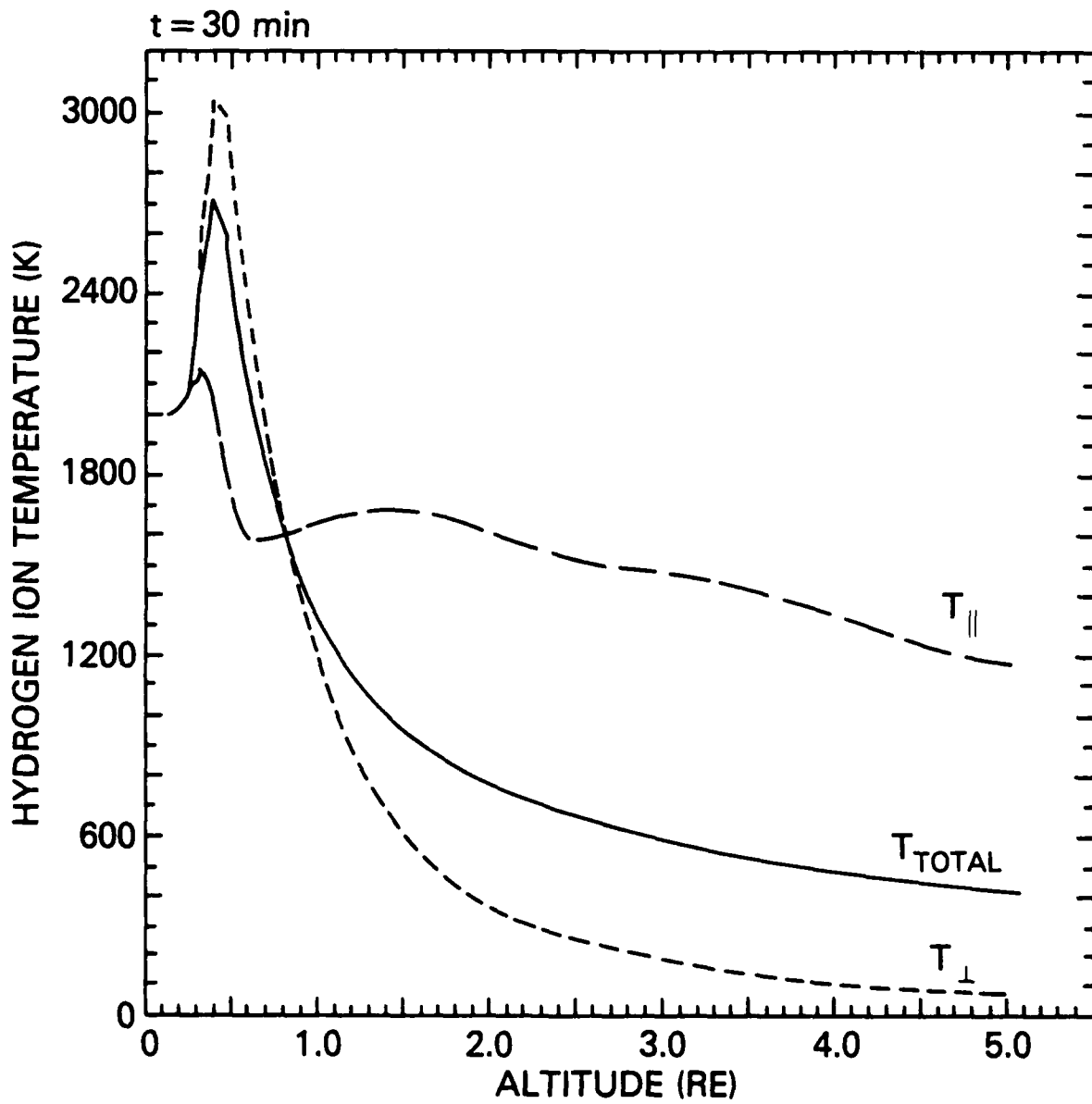


Figure 4. (b) Hydrogen ion temperature 30 minutes after the onset of a current of $-1.0 \mu\text{A}/\text{m}^2$.

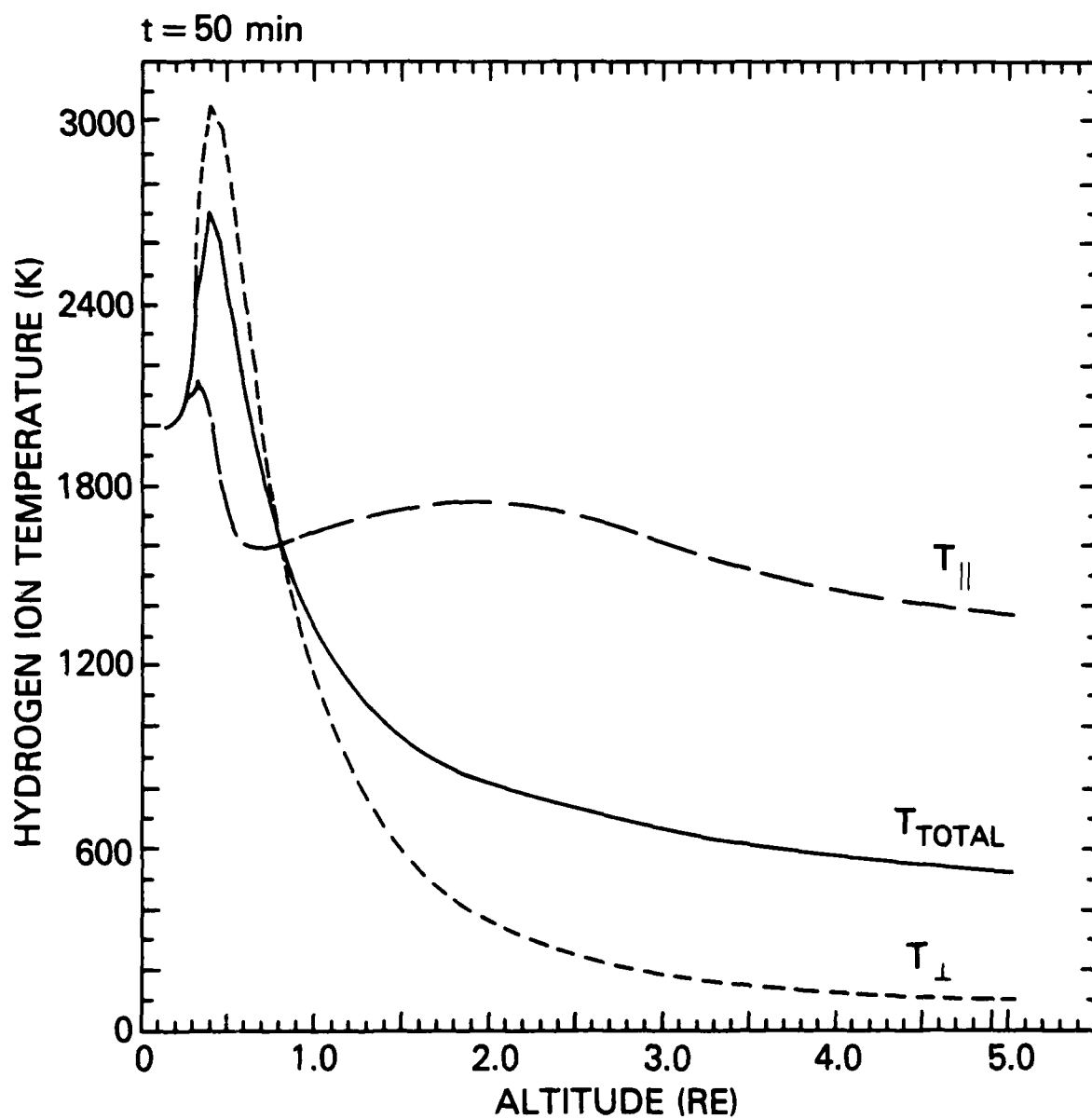


Figure 4. (c) Hydrogen ion temperature 50 minutes after the onset of a current of $-1.0 \mu\text{A}/\text{m}^2$.

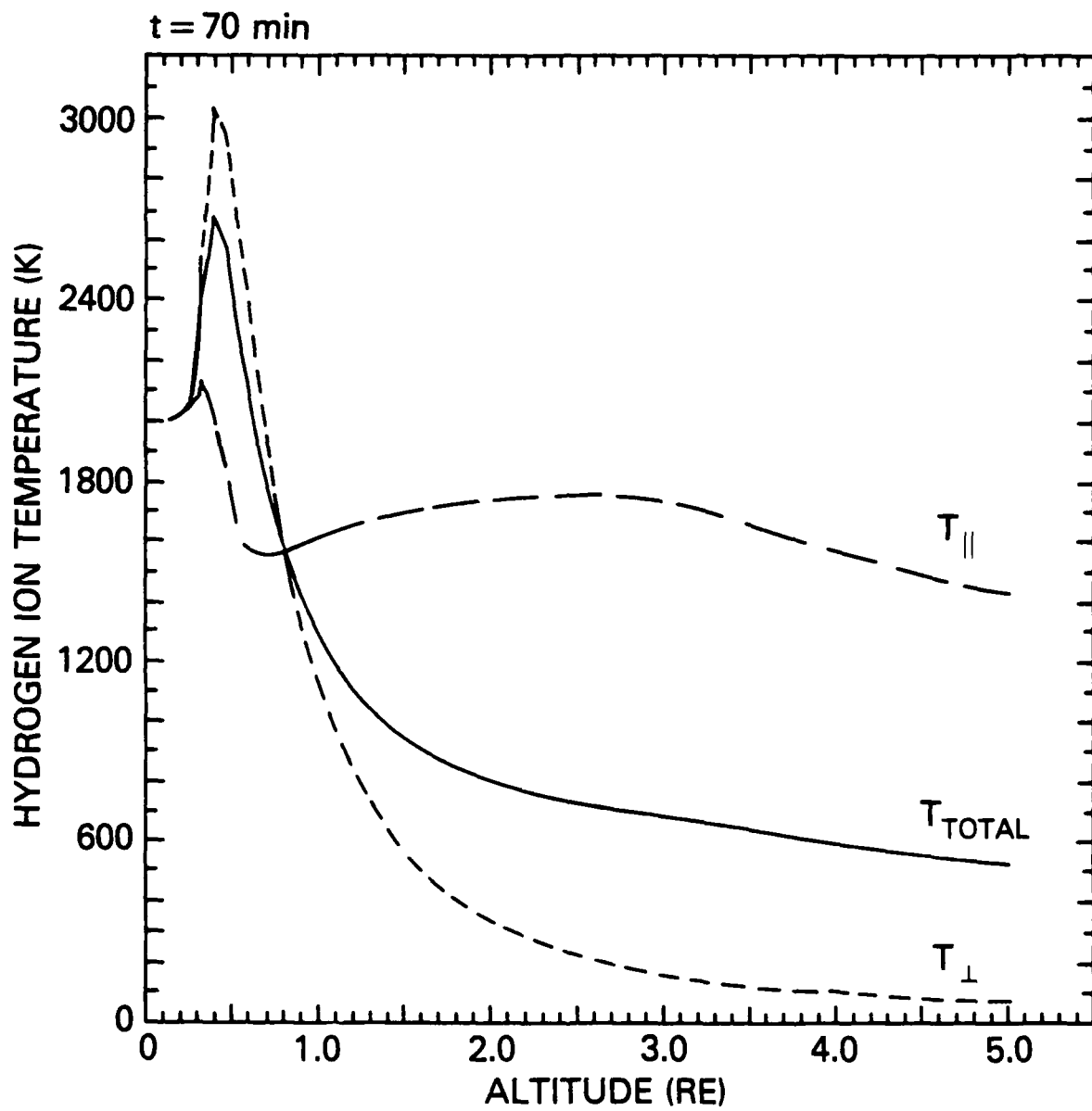


Figure 4. (d) Hydrogen ion temperature 70 minutes after the onset of a current of $-1.0 \mu\text{A}/\text{m}^2$.

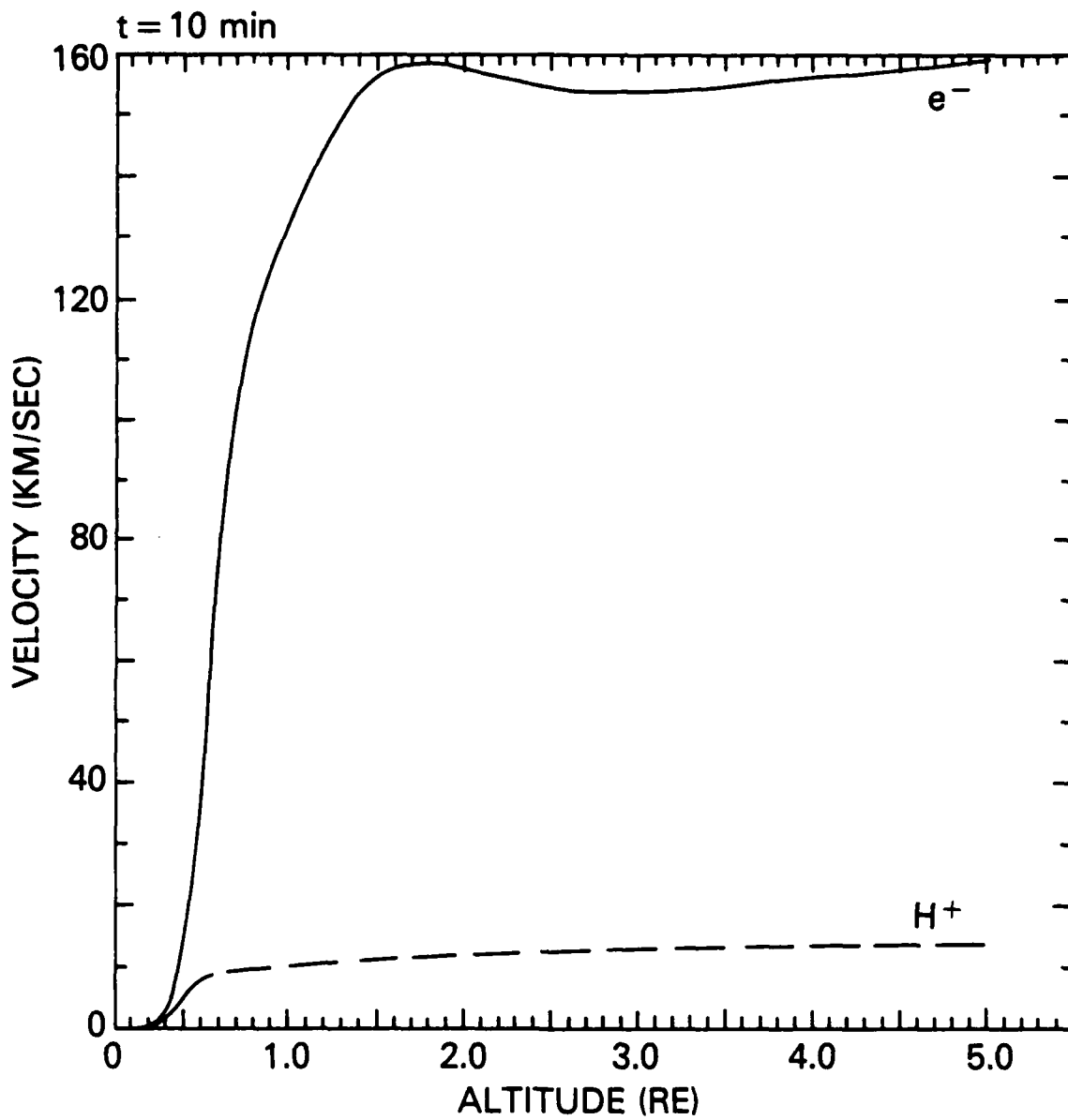


Figure 5. (a) Velocities after 10 minutes after the onset of a current of $-2.0 \mu\text{A}/\text{m}^2$.

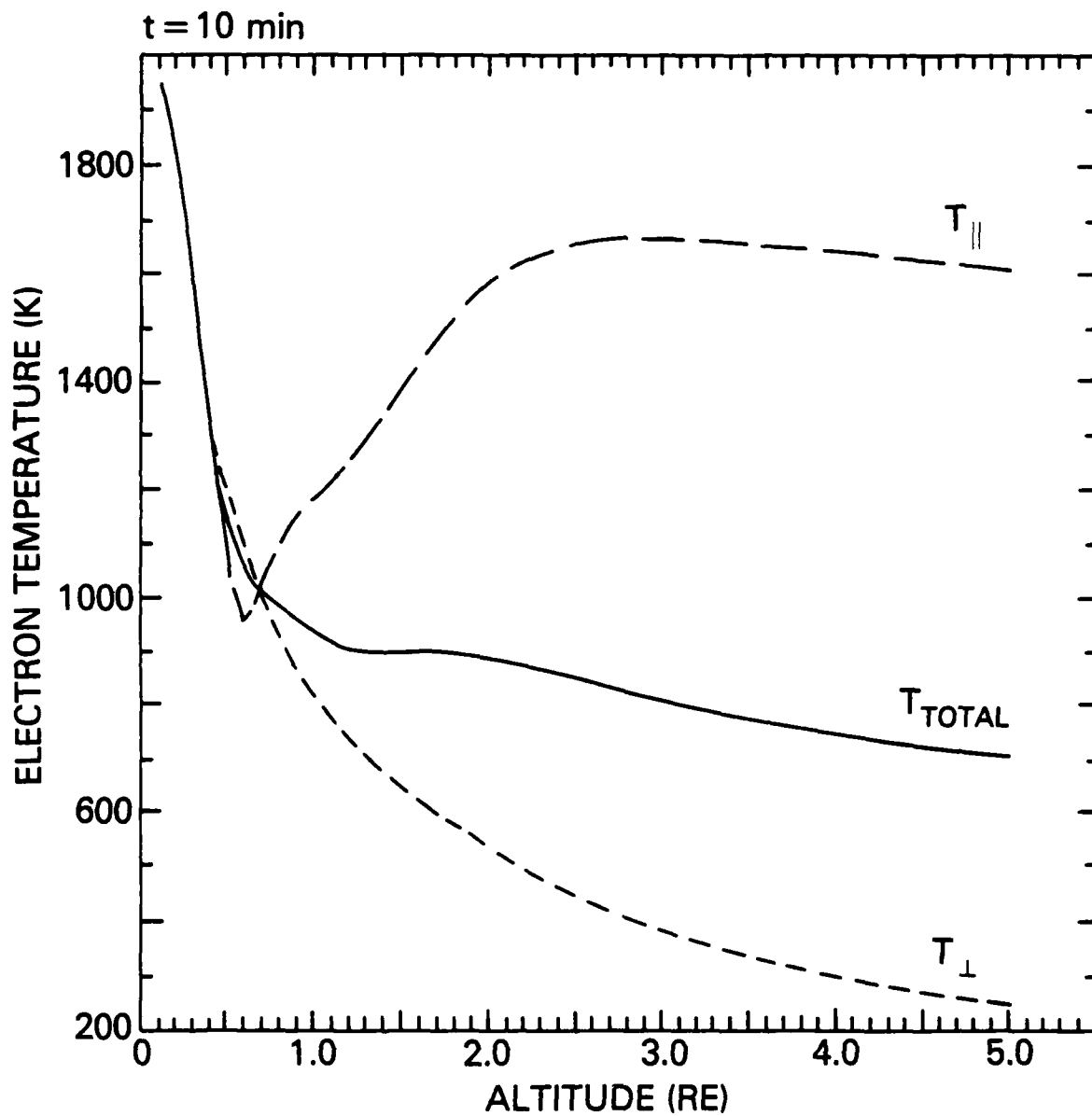


Figure 5. (b) Electron temperature after 10 minutes after the onset of a current of $-2.0 \mu\text{A}/\text{m}^2$.

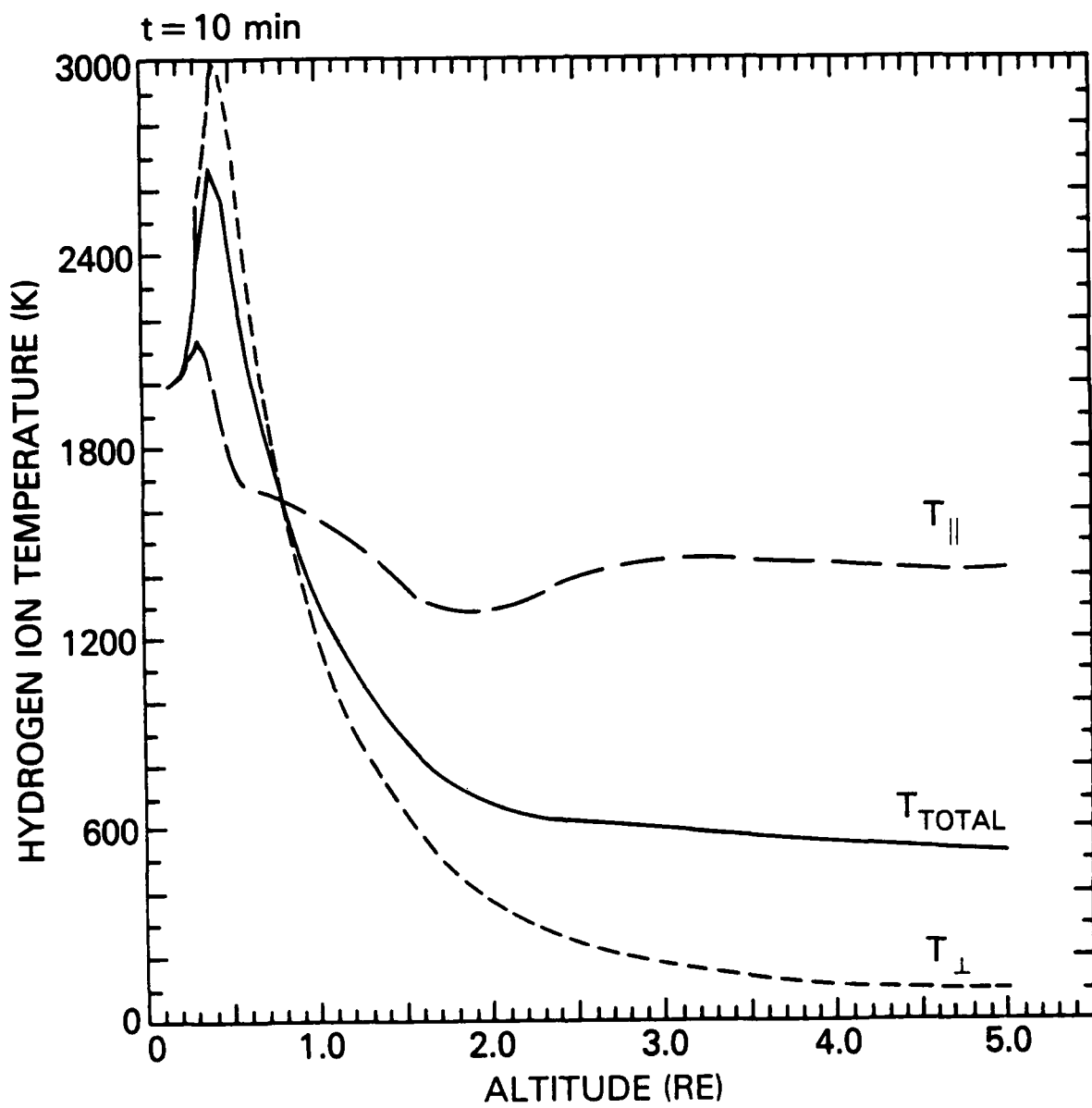


Figure 5. (c) Hydrogen ion temperature after 10 minutes after the onset of a current of $-2.0 \mu\text{A}/\text{m}^2$.

References

- Banks, P.M. and T.E. Holzer, The Polar Wind, *J. Geophys. Res.*, 73, 6846-6854, 1968.
- Banks, P.M. and T.E. Holzer, High-Latitude Plasma Transport: The Polar Wind, *J. Geophys. Res.*, 74 6317-6332, 1969.
- Barakat, A.R., and R.W. Schunk, Transport Equations for Multicomponent Anisotropic Space Plasmas: A Review, *Plasma Physics*, 24, 389-418, 1982.
- Burgers, J.M., Flow Equations for Composite Gases, Academic Press, New York, 1969
- Holtzer, T.E., J.A. Fedder, and P.M. Banks, A Comparison of Kinetic and Hydrodynamic Models of an Expanding Ion-Exosphere, *J. Geophys. Res.*, 76 2453-2468, 1971.
- Iijima, T, and T.A. Potemra, The Amplitude Distribution of Field-Aligned Currents at Northern High Latitudes Observed by Triad, *J. Geophys. Res.*, 81, 2165, 1976.
- Kindel, J.M., and C.F. Kennel, Topside Current Instabilities, *J. Geophys. Res.*, 76, 3055-3078, 1971.
- Lemaire, J., and M. Scherer, Kinetic Models of the Solar and Polar Winds, *Rev. Geophys. Space Phys.*, 11, 427-468, 1973.
- Mitchell, H.G., Jr., and P.J. Palmadesso, A Dynamic Model for the Auroral Field Line Plasma in the Presence of Field-Aligned Current. *J. Geophys. Res.*, 88, 2131, 1983.
- Schunk, R.W., Mathematical Structure of Transport Equations for Multispecies Flows, *Rev. Geophys. Space Phys.*, 15, 429-445, 1977.

Schunk, R.W. and D.S. Watkins, Electron Temperature Anisotropy in the Polar
Wind, J.Geophys. Res., 86, 91-102, 1981.

Schunk, R.W. and D.S. Watkins, Proton Temperature Anisotropy in the Polar
Wind, J.Geophys. Res., 87 171-180, 1982.

APPENDIX

$$\frac{\delta n_b}{\delta t} = 0 \quad (i)$$

$$\frac{\delta v_b}{\delta t} = \sum_a v_b (v_a - v_b) (1 + \phi_{ba}) \quad (ii)$$

$$\begin{aligned} k \frac{\delta T_{b\parallel}}{\delta t} = \sum_a \frac{m_b v_{ba}}{(m_b + m_a)} \left\{ \frac{6}{5} kT_{a\parallel} - \left[2 + \frac{4m_a}{5m_b} \right] kT_{b\parallel} \right. \\ \left. + \frac{4}{5} kT_{a\perp} + \frac{4m_a}{5m_b} kT_{b\perp} + \left[2kT_a + \left(4 + 6 \frac{m_a}{m_b} \right) kT_b \right] \phi_{ba} \right\} \quad (iii) \end{aligned}$$

$$\begin{aligned} k \frac{\delta T_{b\perp}}{\delta t} = \sum_a \frac{m_b v_{ba}}{(m_b + m_a)} \left[3kT_a - 3kT_b + m_a (v_a - v_b)^2 (1 + \phi_{ba}) \right] \\ - \frac{k}{2} \frac{\delta T_{b\parallel}}{\delta t} \quad (iv) \end{aligned}$$

$$\begin{aligned} \frac{\delta q_b}{\delta t} = \sum_a \frac{n_b m_b v_{ba}}{(m_b + m_a)^2} \left[\frac{27}{10} m_a \frac{q_a}{n_a} - \left(3m_b + \frac{8}{5} m_a + \frac{13}{10} \frac{m_a^2}{m_b} \right) \frac{q_b}{n_b} \right. \\ \left. + \frac{3}{2} \frac{m_a}{m_b} (m_a + m_b) kT_b (v_b - v_a) \right] (1 + \phi_{ba}) \quad (v) \end{aligned}$$

Each sum includes all charged particles species in the simulation. the velocity - corrected Coulomb collision frequency ν_{ba} is given by

$$\nu_{ba} = \frac{n_a (32\pi)^{1/2} e_b^2 e_a^2 (m_b + m_a) \ln A \exp(-x_{ba}^2)}{3m_b^2 m_a^3 \alpha_{ba}^3} \quad (\text{vi})$$

($\ln A$ is the Coulomb logarithm), and

$$T_b = \frac{1}{3} T_{b\parallel} + \frac{2}{3} T_{b\perp}$$

$$\alpha_{ba}^2 = \frac{2kT_b}{m_b} + \frac{2kT_a}{m_a}$$

$$x_{ba}^2 = \frac{(v_b - v_a)^2}{\alpha_{ba}^2}$$

$$\phi_{ba} = \frac{2}{5} x_{ba}^2 + \frac{4}{35} x_{ba}^4 + \frac{8}{315} x_{ba}^6$$

Distribution List

Director
Naval Research Laboratory
Washington, D.C. 20375
ATTN: Code 4700 (26 Copies)
Code 4701
Code 4780 (50 copies)
Code 4706 (P. Rodriguez)
Code 2628 (22 copies)

University of Alaska
Geophysical Institute
Fairbanks, Alaska 99701
ATTN: Library
S. Akasofu
J. Kan
J. Roederer
L. Lee
D. Swift

University of Arizona
Dept. of Planetary Sciences
Tucson, Arizona 85721
ATTN: J.R. Jokipii

University of California, S.D.
LaJolla, California 92037
(Physics Dept.):
ATTN: T. O'Neil
J. Winfrey
Library
J. Malmberg
(Dept. of Applied Sciences):
ATTN: H. Booker

University of California
Physics Department
Irvine, California 92664
ATTN: Library
G. Benford
N. Rostoker
C. Robertson
N. Rynn

University of Chicago
Enrico Fermi Institute
Chicago, Illinois 60637
ATTN: E.N. Parker
I. Lerche
Library

University of California
Los Angeles, California 90024
(Physic Dept.):

ATTN: J.M. Dawson
B. Fried
J. Maggs
J.G. Moralles
W. Gekelman
R. Stenzel
Y. Lee
A. Wong
F. Chen
M. Ashour-Abdalla
Library
J.M. Cornwall
R. Walker
P. Pritchett

(Institute of Geophysics and
Planetary Physics):
ATTN: Library
C. Kennel
F. Coroniti

Thayer School of Engineering
Dartmouth College
Hanover, NH 03755
ATTN: Bengt U.O. Sonnerup
M. Hudson

University of Colorado
Dept. of Astro-Geophysics
Boulder, Colorado 80302
ATTN: M. Goldman
Library

Cornell University
School of Applied and Engineering Physics
College of Engineering
Ithaca, New York 14853
ATTN: Library
R. Sudan
B. Kusse
H. Fleischmann
C. Wharton
F. Morse
R. Lovelace
P.M. Kintner

Harvard University
Center for Astrophysics
60 Garden Street
Cambridge, Massachusetts 02138
ATTN: G.B. Field
R. Rosner
K. Tsinganos
G.S. Vaiana

University of Iowa
Iowa City, Iowa 52240
ATTN: C.K. Goertz
D. Gurnett
G. Knorr
D. Nicholson
C. Grabbe
L.A. Frank
K. Nishikawa
N. D'Angelo
R. Merlini
C. Huang

University of Maryland
Physics Dept.
College Park, Maryland 20742
ATTN: K. Papadopoulos
H. Rowland
C. Wu
L. Vlahos

University of Michigan
Ann Arbor, Michigan 48140
ATTN: E. Fontheim

University of Minnesota
School of Physics
Minneapolis, Minnesota 55455
ATTN: Library
Dr. J.R. Winckler
Dr. P. Kellogg
Dr. R. Lysak

M.I.T.
Cambridge, Massachusetts 02139
ATTN: Library
(Physics Dept.):
ATTN: B. Coppi
V. George
G. Bekefi
T. Chang
T. Dupree
R. Davidson
(Elect. Engineering Dept.):
ATTN: R. Parker
A. Bers
L. Smullin
(R.L.E.):
ATTN: Library
(Space Science):
ATTN: Reading Room

Princeton University
Princeton, New Jersey 08540
Attn: Physics Library
Plasma Physics Lab. Library
F. Perkins
T.K. Chu
H. Okuda
H. Hendel
R. White
R. Kurlsrud
H. Furth
S. Yoshikawa
P. Rutherford

Rice University
Houston, Texas 77001
Attn: Space Science Library
T. Hill
R. Wolf
P. Reiff
G.-H. Voigt

University of Rochester
Rochester, New York 14627
ATTN: A. Simon

Stanford University
Radio Science Lab
Stanford, California 94305
ATTN: R. Helliwell

Stevens Institute of Technology
Hoboken, New Jersey 07030

ATTN: B. Rosen
G. Schmidt
M. Seidl

University of Texas
Austin, Texas 78712

ATTN: W. Drummond
V. Wong
D. Ross
W. Horton
D. Choi
R. Richardson
G. Leifeste

Lawrence Livermore Laboratory
University of California
Livermore, California 94551

ATTN: Library
B. Kruer
J. DeGroot
B. Langdon
R. Briggs
D. Pearlstein

Los Alamos National Laboratory
P.O. Box 1663
Los Alamos, New Mexico 87545

ATTN: Library
S.P. Gary
N. Quest
J. Brackbill
J. Birn
J. Borovsky
D. Forslund
J. Kindel
B. Bezzerides
C. Nielson
E. Lindman
L. Thode
D. Winske

Sandia Laboratories
Albuquerque, New Mexico 87115

ATTN: A. Toepfer
D. VanDevender
J. Freeman
T. Wright

Bell Laboratories
Murray Hill, New Jersey 07974

ATTN: A. Hasegawa
L. Lanzerotti

Lockheed Research Laboratory
Palo Alto, California 94304

ATTN: M. Walt
J. Cladis
Y. Chiu
R. Sharp
E. Shelley

Physics International Co.
2400 Merced Street
San Leandro, California 94577

ATTN: J. Benford
S. Putnam
S. Stalings
T. Young

Science Applications, Inc.
Lab. of Applied Plasma Studeis
P.O. Box 2351
LaJolla, California 92037

ATTN: L. Linson

NASA/Goddard Space Flight Center
Greenbelt, Maryland 20771

ATTN: M. Goldstein
T. Northrop
T. Birmingham

NASA/Goddard Space Flight Center
Greenbelt, MD 20771

ATTN: A. Figuero Vinas
Code 692

TRW Space and Technology Group
Space Science Dept.
Building R-1, Room 1170
One Space Park
Redondo Beach, California 90278

ATTN: R. Fredericks
W.L. Taylor

National Science Foundation
Atmospheric Research Section (ST)
Washington, D.C. 20550

ATTN: D. Peacock

Goddard Space Flight Center
Code 961
Greenbelt, Maryland 20771
ATTN: Robert F. Benson

NASA Headquarters
Code EE-8
Washington, D.C. 20546
ATTN: Dr. S. Shawhan
Dr. D. Butler

Klumpar, David
Center for Space Sciences
P.O. Box 688
University of Texas
Richardson, Texas 75080

Aerospace Corp.
A6/2451, P.O. Box 92957
Los Angeles, California 90009
ATTN: A. Newman
D. Gorney
M. Schulz
J. Fennel

Space Science Lab.
University of California
Berkeley, California 94720
ATTN: M. Temerin
F. Mozer

IPST
University of Maryland
College Park, Maryland 20742
ATTN: David Matthews

Utah State University
Dept. of Physics
Logan, Utah 84322
ATTN: Robert W. Schunk

Director
Defense Nuclear Agency
Washington, D.C. 20305
ATTN: Dr. Leon Wittwer
Dr. P. Crowley

Office of Naval Research
Washington, DC 22170
ATTN: Dr. C. Roberson
(Code 412)

Commanding Officer
Office of Naval Research Western
Regional Office
1030 East Green Street
Pasadena, CA 91106
ATTN: R. Brandt

Boston College
Department of Physics
Chestnut Hill, MA 02167
ATTN: R.L. Carovillano
P. Bakshi

University of New Hampshire
Department of Physics
Durham, NH 03824
ATTN: R.L. Kaufmann
J. Hollweg

Director of Research
U.S. Naval Academy
Annapolis, MD 21402 (2 copies)

END

FILMED

1-86

DTIC